Stability, magnetic behavior, and chemical order of $(Co_xFe_{1-x})_N$ ($N=5,13$) nanoalloys

F. Aguilera-Granja
Instituto de Física "Manuel Sandoval Vallarta," Universidad Autónoma de San Luis Potosí, San Luis Potosi 78000, México

A. Vega
Departamento de Física Teórica, Atómica, y Óptica, Universidad de Valladolid, E-47011 Valladolid, Spain
(Received 1 November 2008; revised manuscript received 9 February 2009; published 17 April 2009)

We report a systematic study of the stability, chemical order, and magnetic behavior of free-standing $(Co_xFe_{1-x})_N$ ($N=5$ and 13) nanoalloys as a function of the relative composition in the whole range. Calculations are performed within the *ab initio* density-functional theory (DFT) pseudopotential approximation as implemented in the SIESTA code. Within our DFT approach, the most stable five-atom Fe-Co nanoalloy is found at 40% of Co. A transition from icosahedral to biplanar hcp structure is obtained for $N=13$ as going from the Fe-rich phase to the Co-rich one, although the most stable composition corresponds to pure Co. High average magnetic moments per atom are obtained which decrease, in general, in 1 μ_B/N as increasing the Co concentration due to the substitution of Fe atoms by Co ones having one less *d* hole. Together with this decrease in the average magnetic moment, we find a slight enhancement of the local Co and Fe moments. Our results illustrate the rich structural and magnetic behavior of the Fe-Co alloys at the nanoscale and may be interesting for the design of magnetic grains which could be used in high-density storage devices.

DOI: 10.1103/PhysRevB.79.144423 PACS number(s): 75.75.+a, 36.40.Cg, 75.20.En, 75.50.−y

I. INTRODUCTION

The possibility of designing materials with unique magnetic properties have greatly increased with the potential tailoring of bimetallic transition-metal (TM) nanoparticles which have attracted considerable attention in the last years.[1–3] Although the structural and magnetic properties of pure TM clusters have been widely investigated, very little is still known about the different possible binary clusters, which are the nanometric equivalent to bulk alloys. In general, studies on binary clusters of TM atoms are appealing not only for their possible technological applications in magnetic media or unique catalytic materials but also for theoretical reasons (the computational difficulties which derive from the need to deal with *d* orbitals are even more pronounced for such kind of clusters).

The interaction between the two components of bimetallic clusters introduces a mutual influence on neighboring atoms which leads to the unique properties reported for these nanoalloys. It has been clearly established, both experimentally and theoretically, that the properties of binary nanoalloys are not necessarily given by the average behavior of their corresponding isolated constituents and that the observed phenomena strongly depend on the precise details of their geometry and composition.[4–7] A deep understanding of the geometrical structure, chemical order, and electronic properties as a function of the composition is of fundamental importance in order to fabricate TM alloyed nanoparticles for atomic engineering of the nanostructured materials for the future.

In the bulk regime, pure Co and Fe are the ferromagnetic elements with the higher magnetic moments. Moreover, their intermetallic bulk alloy with a Co concentration of 30% is known to exhibit the largest bulk magnetic moment of ≈ 2.45 μ_B.[8] The magnetic moment is expected to be enhanced at the nanoscale due to finite size effects, one of the most technologically important features. However, the structural and magnetic properties of Co-Fe nanoalloys in the form of isolated clusters with different relative concentrations have not received similar attention as their bulk counterpart. It is the aim of the present work to shed light on this open question.

From the structural point of view, the problem is not simple. Both Fe and Co have almost the same atomic size and similar surface energies, as a consequence of which it is not obvious to predict the existence of surface segregation in favor of one particular species upon alloying. Moreover, their bulk structures are different (bcc for Fe and hcp for Co). It is worth to comment that even if in bimetallic nanoparticles it is experimentally possible to identify the type and the relative composition of the species involved, nowadays there is no experimental technique capable of accurately determining the local geometrical and chemical structure in these kind of nanoalloys, a fact that seriously limits the understanding of the measured data. The structures of finite clusters are in general not the same as in their bulk counterparts.

In the present work, we have selected two sizes for the Co-Fe nanoalloys, $N=5$ and $N=13$ to calculate, using the density-functional theory (DFT), the magnetic behavior and the chemical order as a function of the relative concentration of the two ferromagnetic elements. The size $N=5$ is small enough to have only surface atoms, and all previous studies the ground state of pure Fe_5 and Co_5 clusters give a trigonal bipyramid structure for the ground state. The size $N=13$ is big enough to contain not only surface atoms but also a core with one atom. Moreover, since different geometries have been proposed for the pure Fe_{13} and Co_{13} clusters, a structural transition is expected in the $N=13$ nanoalloy as a function of the concentration. The theoretical study of these small binary nanoparticles can be also interesting in the context of high-density magnetic recording, where the design of molecular magnets to be used as magnetic bits is an important goal. One way to increase the density of recording is to de-

TABLE I. Average magnetic moment per atom, binding energy, and average interatomic distance of pure Fe_N clusters ($N=2,3,5,13$) calculated through different DFT approaches together with ours.

Size	Structure	$\bar{\mu}$ μ_B	Energy (eV/atom)	Average distance (Å)	Method
2	Pair	3.00	1.317	2.03	This work SIESTA-GGA
		3.00	2.25	1.96	SIESTA-LSDA[b]
		3.00		1.95	deMon-KS GGA[c]
				1.95	deMon-KS LSDA[c]
		3.00	1.599	2.02	DMOL-BLYP[d]
			1.30	1.87–2.02	Exp.[e,f]
3	Triangle	3.33	1.770	2.29	This work SIESTA-GGA
		3.33	1.942		DMOL-BLYP[g]
		2.70		2.10	deMon-KS GGA[c]
				2.10	deMon-KS LSDA[c]
		2.67	2.67	2.14	SIESTA-LSDA[b]
5	Trigonal BP	3.60	2.534	2.45	This work SIESTA-GGA
		3.20			VASP-GGA[h]
		3.60			GAUSSIAN-B3LYP[a]
		3.20	2.549		DMOL-BLYP [d]
		3.20		2.33	deMon-KS GGA[c]
13	ICO	3.38	3.410	2.57	This work SIESTA-GGA
	HCP	3.08	3.287	2.52	This work SIESTA-GGA
	ICO	3.38	3.086		DMOL-BLYP[d]
	3D HCP	3.08	3.023		DMOL-BLYP[d]
	ICO	3.38			VASP-GGA[h]
	ICO	2.62	4.43	2.48	SIESTA-LSDA[b]
	3D HCP	2.46	4.31		SIESTA-LSDA[b]

[a]Reference 8.
[b]Reference 14.
[c]Reference 15.
[d]Reference 16.
[e]Reference 17.
[f]Reference 18.
[g]Reference 19.
[h]Reference 20.

crease the size of the particles which will be placed on the substrate.

The rest of the paper is organized as follows. In Sec. II we briefly describe the theoretical model and approximations used for the calculations. In Sec. III we benchmark our theoretical approach against previous calculations in the case of pure Fe and Co clusters of sizes $N=2$, 3, 5, and 13. Section IV is devoted to the $N=5$ and $N=13$ CoFe nanoalloys. The main conclusions are summarized at the end.

II. DETAILS OF THE COMPUTATIONAL PROCEDURE

We have obtained the structural and electronic properties of our clusters by means of DFT calculations using numerical atomic orbital basis and pseudopotentials to solve the single-particle Kohn-Sham (KS) equations as implemented in the SIESTA code.[9] For the exchange-correlation potential we have used the Perdew, Burke, and Ernzerhof (PBE) version[10] of the generalized gradient approximation (GGA). We have replaced the atomic cores by nonlocal, norm-conserving Troullier-Martins pseudopotentials[11] that were factorized in the Kleinman-Bylander form,[12] and we have included nonlinear core corrections to account for the significant overlap of the core charge with the valence $3d$ orbitals. The ionic pseudopotentials have been generated using the atomic configurations: $3d^8\ 4s^1$ for Co and $3d^7\ 4s^1$ for Fe. Previous studies of Fe in different environments suggest this configuration as adequate for building a transferable pseudopotential.[13] The core radii were $2au$ for the s, p, and d orbitals of both Fe and Co. We have represented the valence states using double-ζ basis sets with two orbitals having different radial forms to describe both the $4s$ and $3d$ states of Co and Fe, and one orbital to describe the $4p$ states. We have considered a 22 $Å^3$ supercell and used a 200 Ry energy cutoff to define the finite real-space grid for numerical integrations. We have allowed the clusters to relax without any symmetry (or spin) constraints using a gradient conjugate algorithm until the interatomic forces were smaller than 0.005 eV/Å. For certain clusters, we have performed additional calculations increasing the accuracy (in both the electronic self-consistency and the calculation of forces) and considering also a larger mesh cutoff to define the real-space grid for numerical calculations (up to 300 Ry) as well as a more extended basis.

TABLE II. Average magnetic moment per atom, binding energy, and average interatomic distance of pure Co_N clusters ($N=2,3,5,13$) calculated through different DFT approaches together with ours.

Size	Structure	$\bar{\mu}$ μ_B	Energy (eV/atom)	Average distance (Å)	Method
2	Pair	2.00	1.449	2.01	This work SIESTA-GGA
		2.00	1.452	1.96	VASP-GGA[d]
		2.00	2.539	2.14	DMOL-BLYP[c]
				1.96	VASP-GGA[e]
		2.50	1.425	2.04	Amsterdam DF code[f]
		2.00		1.95	deMon-KS GGA[b]
				1.92	deMon-KS LSDA[b]
			1.32–1.72	2.31	Exp.[g],[h]
3	Triangle	2.33	1.885	2.24	This work SIESTA-GGA
		2.33	1.783	2.19	VASP-GGA[d]
		2.33	2.883	2.14	DMOL-BLYP[c]
		2.33	1.800	2.28	ADF[f]
		1.67		2.24	deMon-KS GGA[b]
				2.18	deMon-KS LSDA[b]
			1.32–1.72	2.31	Exp.[g],[h]
			1.45–		Exp.[i]
5	Trigonal BP	2.60	2.667	2.43	This work SIESTA-GGA
		2.60	2.553	2.34	VASP-GGA[d]
		2.20			GAUSSIAN-B3LYP[a]
		2.60	2.160	2.29	ADF[f]
		1.80		2.29	deMon-KS GGA[b]
			2.840		Exp.[i]
13	HCP	2.08	3.501	2.42	This work SIESTA-GGA
	ICO	2.38	3.432	2.49	This work SIESTA-GGA
	HCP	2.08	5.260	2.34	VASP-GGA[e]
	ICO	2.38	5.134		VASP-GGA[e]
	3D HCP	1.92	3.279		VASP-GGA[d]
	ICO	2.38	3.266		VASP-GGA[d]
		2.00 ± 0.06			Exp.[j]
		2.30 ± 0.07			Exp.[k]

[a]Reference 8.
[b]Reference 15.
[c]Reference 19.
[d]Reference 21.
[e]Reference 22.
[f]Reference 23.
[g]Reference 24.
[h]Reference 25.
[i]Reference 26.
[j]Reference 27.
[k]Reference 28.

III. RESULTS FOR PURE FE AND CO CLUSTERS

In order to test our theoretical method we have performed calculations for pure Fe_N and Co_N clusters with $N=2$, 3, 5, and 13, and we have compared our results with other DFT calculations as well as with experiments from other groups, available in the literature. All the results are presented in Tables I and II for the Fe_N and Co_N clusters, respectively. Our calculations give the same ground-state geometry as the other DFT calculations for all the pure clusters investigated.

For the dimers, all calculations give the same average magnetic moment per atom and similar interatomic distances (comparable with the experimental ones for Fe_2 but underestimated for Co_2). Our binding energies compare well with the experimental ones as well as with those obtained with other DFT-GGA methods, but for Fe_2 they are smaller, as expected, than those obtained with SIESTA-LSDA (local spin density approximation) and for Co_2 they are smaller than those obtained with DMOL-BLYP.

For the triangles, there is more dispersion in the results of different DFT approaches. In general, the GGA calculations lead to higher magnetic moments and lower binding energy than the LSDA ones. Again, the DMOL-BLYP calculation gives much larger binding energies than the rest of DFT calculations, in particular for Co_3.

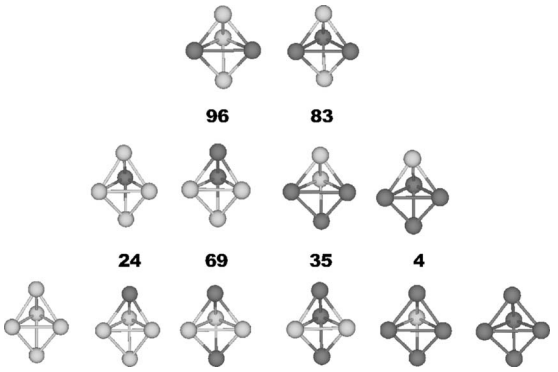

FIG. 1. Illustration of the different homotopes (trigonal BP) of the five-atom CoFe nanoalloy as a function of the relative composition. Dark gray balls represent the Co atoms, while light gray ones represent the Fe atoms. Each column contains the different homotopes of a given composition. The lowest energy homotopes are at the bottom row. For each column concentration, the energy differences per atom with respect to the lowest energy homotome are given.

For the five-atom clusters with trigonal bipyramid (trigonal BP) structure, there is less dispersion in the results of the different methods. High average moments are reported for Fe_5 (with differences of 0.40 μ_B/atom). For Co_5, all calculations give a high moment of 2.60 μ_B/atom except those using Gaussian-B3LYP and deMon-KS GGA which lead to lower moments.

Finally for the 13-atom clusters, all calculations agree in the icosahedral (ICO) structure as the ground state of Fe_{13} and in the hcp-like (HCP) one as the ground state of Co_{13}. In view of this result, we checked these two structures in both Fe_{13} and Co_{13}. In Fe_{13}, all calculations give similar magnetic moments for both structures, except SIESTA-LSDA; it gives lower moments and larger binding energies, as usual. In Co_{13} all calculations give similar magnetic moments. It is worth noting that the two different experimental results available for Co_{13} give different values for the average moment per atom, one of which corresponds with the theoretical predictions for the HCP structure whereas the other one is closer to the theoretical predictions icosahedral for ICO structure.

In resume, we can conclude that our DFT approach leads to a good overall agreement with the other methods as well as with experiments (when available) for the pure Fe and Co clusters, with regard to the binding energies, magnetic moments, and interatomic distances. This indicates, in particular, that our double-ζ basis sets are sound enough and that our pseudopotentials are transferable from the isolated atom to the cluster environment. Therefore, this gives us confidence in the accuracy of our method for the study of nanoalloys of similar sizes.

IV. RESULTS FOR THE CoFe NANOALLOYS

For both the pure Fe_5 and Co_5 clusters, the trigonal bipyramid is the ground-state structure as discussed in Sec. III, and therefore this structure is considered for our $(Co_xFe_{1-x})_5$ nanoalloys. For this size the number of different homotopes

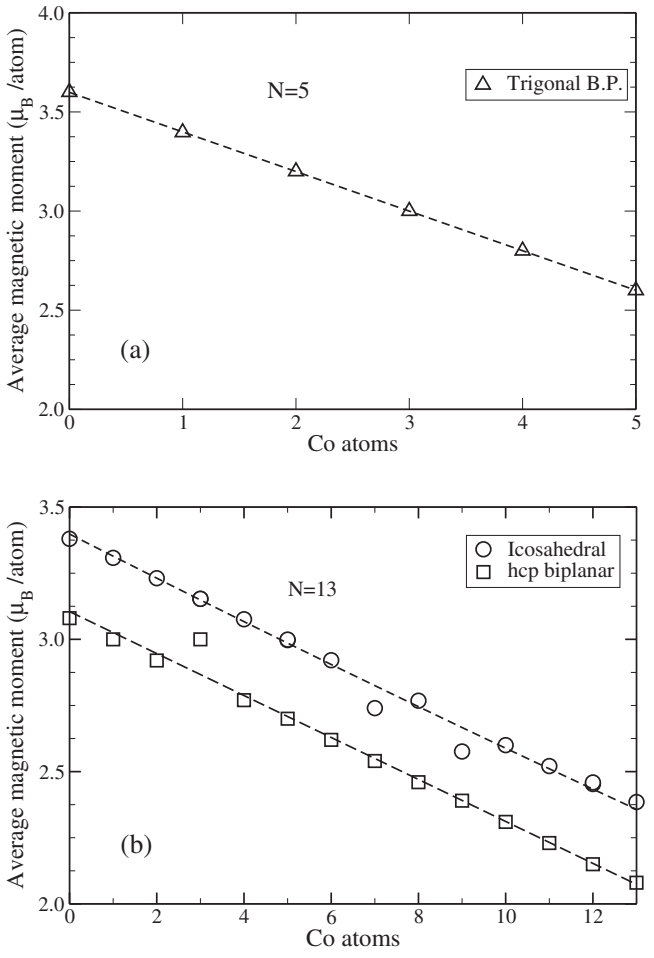

FIG. 2. Average magnetic moment per atom (in units of μ_B) of the lowest energy homotopes of the 5-atom (a) and 13-atom icosahedral and biplanar hcp (b) CoFe nanoalloys as a function of the number of Co atoms. The lines mark the perfect 1 μ_B/N decreasing behavior.

for each relative composition is small and we have calculated all of them. These are illustrated in Fig. 1. This nanoalloy has been previously investigated by Mpourmpakis *et al.*[8] using the GAUSSIAN code with a hybrid functional B3LYP. We obtain the same chemical order as them for the lowest energy isomers of different compositions except for Co_3Fe_2 and Co_4Fe_1. In this Co-rich phase, they find the equator of the bipyramid filled by Co atoms, whereas in our case Co atoms prefer to have low coordination of Co which is the trend obtained through both SIESTA-GGA and GAUSSIAN-B3LYP calculations in the Fe-rich phase. In the case of Co_4Fe_1, both homotopes are nearly degenerated in our SIESTA-GGA calculation (see Fig. 1). Our SIESTA-GGA average interatomic distances are slightly smaller (between 5% and 10%) than those obtained with GAUSSIAN-B3LYP.[8]

With regard to the average magnetic moment per atom as a function of the relative composition we obtain high values, in the saturation limit, which decrease in 1 μ_B/N (N=5 for this size) as a function of the Co concentration for each Co atom substituting an Fe one [see Fig. 2(a)]. Typically, the nonmonotonic behavior of the average magnetic moment of free ferromagnetic transition-metal clusters as a function of

the cluster size is due to changes in the structural symmetry and/or to relaxations which strongly modify the electronic structure of certain clusters. In binary clusters containing transition-metal elements of the middle of the $3d$ row, changes in the structure or in the stoichiometry could lead also to antiparallel or to noncollinear magnetic couplings (due to magnetic frustrations) accompanied by a reduction (or quenching) in their average moments. In all FeCo nanoalloys studied in the present work, the magnetic coupling is parallel (ferromagneticlike), independently of the stoichiometry. This is not surprising for late transition-metal elements such as Fe and Co. In addition, all the homotopes have a trigonal bipyramid structure (same symmetry) and the average interatomic distance in the clusters does not depend on the relative composition (the differences do not exceed 0.03 Å). Therefore, the 1 μ_B/N decrease in the average moment as increasing the Co concentration is due essentially to the fact that Co has one d hole less than Fe in the d band. This 1 μ_B/N decrease in the average magnetic moment has been previously reported by Mpourmpakis *et al.*[8] for different small CoFe nanoalloys. But in the particular case of $(Co_xFe_{1-x})_5$, their results deviate from this trend since they find a jump (with a decrease larger than 1 μ_B/N) from Co_2Fe_3 to Co_3Fe_2. In the Fe-rich phase we obtain the same values for the magnetic moments as those reported by Mpourmpakis *et al.*[8] In the Co-rich phase, however, we predict larger values due to our larger predicted Co magnetic moment. For Co_5 we have 2.60 μ_B instead of their 2.20 μ_B, and this tendency also holds for the homotopes in the Co-rich phase. Note that for the pure clusters (discussed in the previous section), the GAUSSIAN-B3LYP of Mpourmpakis *et al.*[8] gave similar magnetic moments as SIESTA-GGA for Fe_5 but lower magnetic moments than most of previous DFT calculations for Co_5. This could indicate that the hybrid B3LYP functional slightly underestimates in general the magnetic moment of Co.

Let us now discuss some additional trends obtained in our calculations. In Fig. 3(a) we plot the binding energy as a function of the Co concentration. The binding energy is calculated as the sign reversed difference between the energy of the cluster and the sum of the energies of each individual constituent atom. Within our DFT approach, the most stable five-atom Fe-Co nanoalloy has 40% of Co. It is not easy to define the kind of chemical order (segregated or mixed) of the five-atom nanoalloy due to its finite and small size. In order to analyze qualitatively these trends as a function of the relative composition, it is convenient to define an order parameter, σ, with the following characteristics: positive when phase separation (segregation) takes place, close to zero when mixing together with disorder happens, and negative when layerlike order is presented. This parameter is usually employed in bulklike systems.[29] The σ parameter is defined as

$$\sigma = \frac{N_{\text{Co-Co}} + N_{\text{Fe-Fe}} - N_{\text{Co-Fe}}}{N_{\text{Co-Co}} + N_{\text{Fe-Fe}} + N_{\text{Co-Fe}}}, \quad (1)$$

where N_{ij} (with i and j=Co and Fe) is the number of nearest-neighbors i-j bonds. The number of these different kinds of bonds corresponds to the multiplicities given in parenthesis

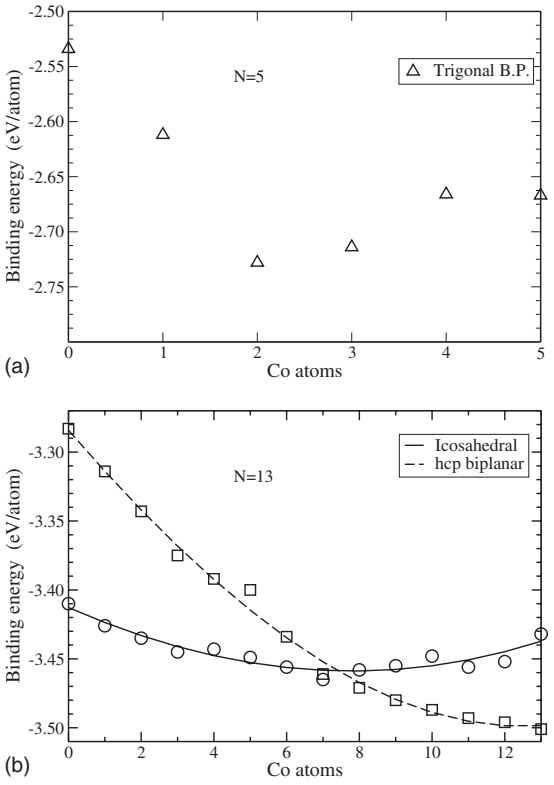

FIG. 3. Binding energy per atom of the lowest energy homotopes of the 5-atom (a) and 13-atom icosahedral and biplanar hcp (b) CoFe nanoalloys as a function of the number of Co atoms. The curves are a fit to the data as guide to the eyes.

in Table III. The average interatomic distances for the different kinds of pairs within the clusters are also reported in Table III. Our results for σ in the five-atom nanoalloy as a function of the Co concentration are shown in Fig. 4(a). We see a tendency to segregate for both the low and the rich Co concentrations and a slight tendency to mix for the intermediate concentration region. A better understanding of the chemical order behavior will be achieved after the analysis of the 13-atom Co-Fe nanoalloy later on.

Coming now to the local properties, a very interesting magnetic behavior comes out. Despite the 1 μ_B/N decrease of the average magnetic moment per atom in this nanoalloy (N=5) as increasing the Co concentration (due to the substitution of Fe atoms by Co ones), we find a slight enhancement of both the Co and the Fe average magnetic moments (see Table III). The system becomes slightly more magnetic locally since in general the local moments at both the Co and Fe sites enhance as increasing the Co concentration. We obtain a slight charge transfer from the $3d$ states toward the sp ones in both Co and Fe. This charge transfer increases as increasing the Co concentration, thus working in favor of the enhancement found in the local moments. We have performed the calculations for the Co-Fe dimer, and we have found the similar trend as in the five-atom nanoalloys. Thus, the local Fe moment increases from 3 to 3.16 μ_B as going from Fe_2 to CoFe and the Co moment increases from 1.83 to 2 μ_B as going from CoFe to Co_2. Moreover, the binding energy of the CoFe dimer (1.512 eV/atom) and its inter-

TABLE III. Average homonuclear and heteronuclear interatomic distances (in angstrom) and average Co and Fe magnetic moments (in μ_B) of the lowest energy homotopes of the five-atom CoFe nanoalloys as a function of the number of Co atoms. In parenthsis is shown the number of nearest neighbors bonds.

Co atoms	Co-Co	Fe-Fe	Co-Fe	μ(Co)	μ(Fe)
0		2.448(9)			3.60
1		2.507(6)	2.319(3)	2.32	3.67
2		2.638(3)	2.306(6)	2.37	3.75
3	2.252(2)	2.527(1)	2.457(6)	2.47	3.79
4	2.358(5)		2.492(4)	2.55	3.80
5	2.426(9)			2.60	

atomic distance (1.97 Å) are, respectively, larger and smaller than the values obtained in both homonuclear dimers (see Tables I and II to compare). This indicates that the heteronuclear bonding in these nanoalloys is strong and it is accompanied by a slight increase in the local spin polarization.

Let us discuss now the $(Co_xFe_{1-x})_{13}$ nanoalloy. For this size, the structural ground states of the pure Fe_{13} and Co_{13} clusters are different as discussed in Sec. III. Fe_{13} is an icosahedron whereas Co_{13} is a biplanar hcp. It is expected that a structural transition will take place at a certain relative composition of the nanoalloy, and therefore we have investigated both structures in the whole range of concentrations. In Fig. 5 we show our predicted lowest energy homotopes for the different relative compositions in the two structures. The number of possible different homotopes in this case is much larger than for $N=5$, in particular at the intermediate concentrations, as a consequence of which we used the following strategy of search. For concentrations $x<0.24$ and $x>0.76$ we considered as input all the possible homotopes. For inter-

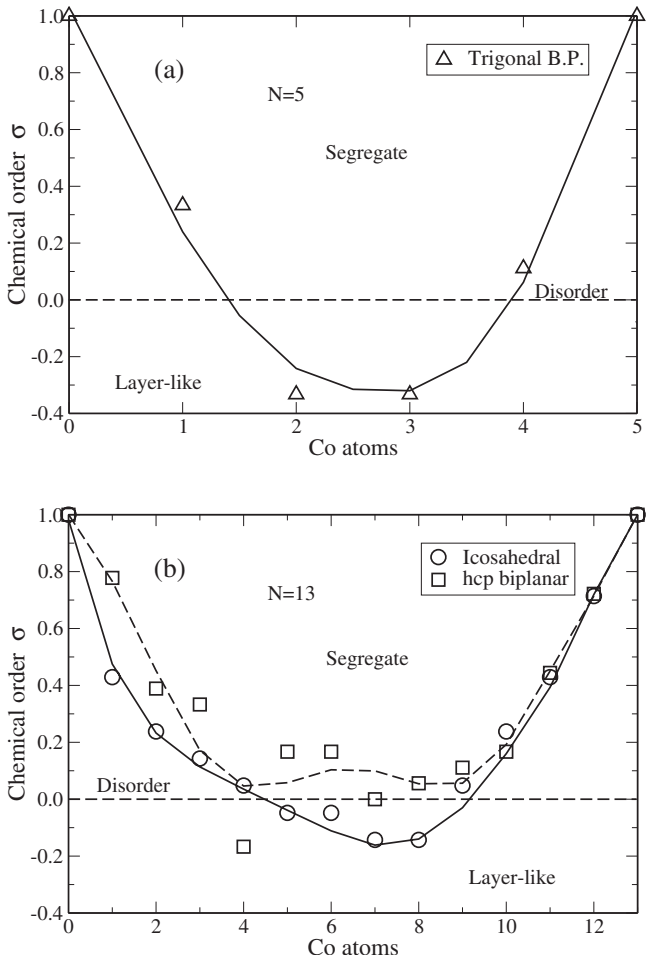

FIG. 4. Chemical order parameter σ, as defined in the text, of the lowest energy homotopes of the 5-atom (a) and 13-atom icosahedral and biplanar hcp (b) CoFe nanoalloys as a function of the number of Co atoms. The curves are a fit to the data as guide to the eyes.

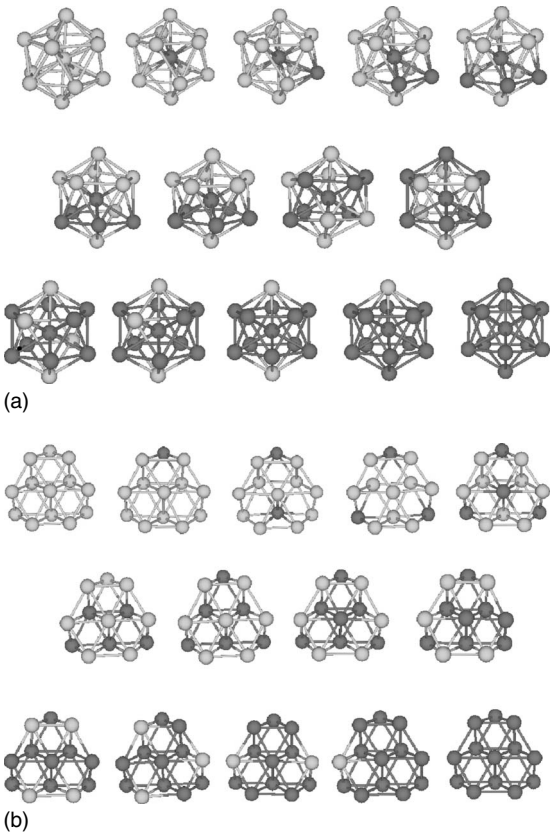

FIG. 5. Illustration of the lowest energy homotopes of the 13-atom CoFe nanoalloy with icosahedral (upper part) and biplanar hcp (lower part) structures as a function of the relative composition. Dark gray balls represent the Co atoms, while light gray ones represent the Fe atoms.

mediate concentrations, $0.24 \leq x \leq 0.76$, we endeavored to test enough number of different homotopes of mixed, segregated and layerlike ordering type as well as with preference of Co or Fe for the central site in the icosahedral structure. For the icosahedral structure, the lowest energy homotopes found in the dilute limits allowed us to find the tendency of Co to occupy the central site and the tendency of Fe to locate itself at the surface. A growth pattern was obtained at the initial stages of increasing Co concentration (the formation of a pentagonal pyramid subcluster); we verified it by considering homotopes in which the Co atoms did not form such subcluster and lost the segregated character. This type of growth changed for $x=7$ at which the pentagonal pyramid subcluster of Co was filled. Around this concentration we tested more different inputs and we found the growth of a central Co subcluster. For the intermediate concentrations ($0.24 \leq x \leq 0.76$) we tested 63 different homotopes. No clear trends came out, however, for the hcp biplanar structure which does not have a central site. Therefore, a more exhaustive search was carried out in the intermediate concentrations range in this case by considering 96 different homotopes as input, that is, ≈50% more than for the icosahedral family. We note, however, that since we have not tested all possible homotopes for the intermediate concentrations, we cannot guarantee that our predicted lowest energy homotopes for $0.24 \leq x \leq 0.76$ are the ground state. The average interatomic distance decreases (quasilinearly) from (2.57 Å) 2.53 Å to 2.49 Å (2.42 Å) for the icosahedral (hcp) nanoalloys, as going from pure Fe character to pure Co character.

The results for the average magnetic moments per atom [Fig. 2(b)] indicate, as in the five-atom nanoalloy, a decrease in 1 μ_B/N ($N=13$ for this size) as a function of the Co concentration, except for some particular cases. For the icosahedral structure, we find a decrease larger than 1 $\mu_B/13$ for Co_7Fe_6 and Co_9Fe_4, although for Co_9Fe_4 there is a spin isomer which follows the linear behavior and whose binding energy is only 0.002 eV lower. If we consider that both are degenerated, only Co_7Fe_6 clearly departs from the linear behavior, and we note that it corresponds exactly with the Co concentration for which the growth pattern changes ($x=7$). For the hcp structure, Co_3Fe_{10} has an average moment which lies above the linear trend. It is worth noting that in this configuration Co minimized the Fe coordination and maximized the Co-Co interatomic distance. The icosahedral nanoalloy has larger spin polarization, and closer to the saturation, than the hcp one. At a given composition, the icosahedral nanoalloy has slightly larger average interatomic distance and larger number of bonds than the hcp one. Larger interatomic distances work in favor of magnetism while larger coordination works against it. In view of our results, the former effect dominates.

The binding energy as a function of Co concentration is plotted in Fig. 3(b) for the two structures of the $(Co_xFe_{1-x})_{13}$ nanoalloy. As expected, we predict a structural transition from the icosahedral structure to the hcp one. For low and intermediate Co concentration the icosahedral structure is more stable than the biplanar hcp structure, while for high Co concentrations (higher than about $x \approx 0.5-0.6$) the energetic order reverses. Taking into account that hcp nanoalloys are less magnetic than icosahedral ones, together with the decrease in the average moment as increasing the Co concentration, going beyond $x \approx 0.54$ will reduce the performance of the nanoalloys from the magnetic point of view. However, we note that due to the icosahedral to hcp structural transition together with the monotonous energy gain in the hcp structure as increasing the Co concentration, the most stable composition corresponds to the pure Co_{13} instead of Co_7Fe_6 which would be the most stable nanoalloy if the icosahedral structure was preserved.

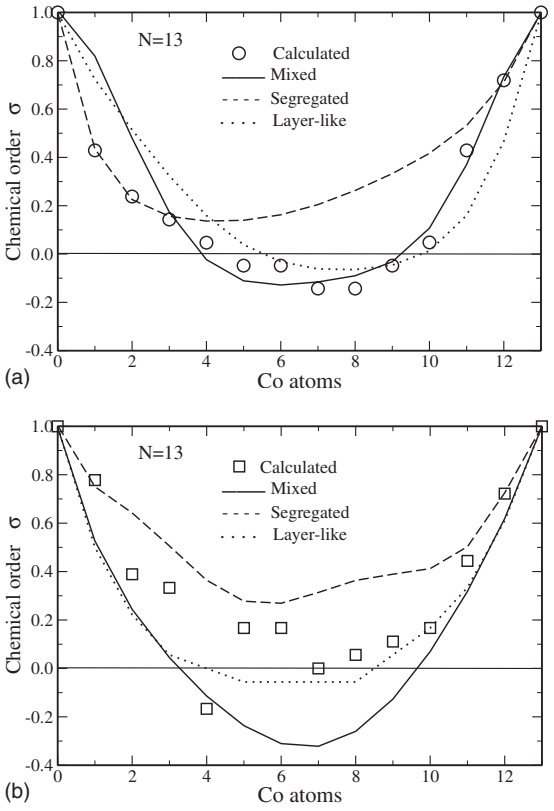

FIG. 6. Chemical order parameter σ of the lowest energy homotopes of the icosahedral (a) and hcp biplanar (b) 13-atom CoFe nanoalloys as a function of the number of Co atoms. Solid, dashed, and dotted curves correspond to the model of ideal mixed, segregated, and layerlike nanoalloys, respectively, as explained in the text.

With regard to the segregated or mixed character of the 13-atom nanoalloys, we plot in Fig. 4(b) the chemical order parameter σ for the two structures. Although we obtain a similar overall behavior as in the smaller five-atom nanoalloy, it is interesting to analyze the differences between the icosahedral and the hcp structures. We observe that independent of the relative composition, the biplanar hcp nanoalloys have more tendency to segregation than the icosahedral ones. To better interpret the kind of chemical order, we compared in Fig. 6 the results of the σ parameter of Fig. 4(b) with three ideal model curves for the mixed, segregated, and layerlike orderings in the nanoalloys. For these model curves, we calculated σ in ideal (bulk distances) 13-atom clusters with either icosahedral and biplanar hcp structures choosing only those arrangements that maximized the three types of chemical orders. The icosahedral nanoalloys are clearly segregated at low Co concentrations, and this is reflected in the distri-

TABLE IV. Average homonuclear and heteronuclear interatomic distances (in angstrom) and average Co and Fe magnetic moments (in μ_B) of the lowest energy homotopes of the icosahedral 13-atom CoFe nanoalloys as a function of the number of Co atoms. In parenthesis is shown the number of neighbors bonds.

Co atoms	Co-Co	Fe-Fe	Co-Fe	μ(Co)	μ(Fe)
0		2.571(42)			3.38
1		2.584(30)	2.457(12)	1.76	3.44
2	2.443(1)	2.594(25)	2.496(16)	1.98	3.46
3	2.530(3)	2.592(21)	2.485(18)	2.09	3.47
4	2.540(5)	2.602(17)	2.486(20)	2.13	3.49
5	2.503(7)	2.603(13)	2.505(22)	2.19	3.51
6	2.493(10)	2.618(10)	2.498(22)	2.21	3.53
7	2.523(12)	2.753(6)	2.456(24)	2.09	3.41
8	2.518(15)	2.685(3)	2.495(24)	2.26	3.58
9	2.495(20)	2.760(2)	2.515(20)	2.17	3.49
10	2.491(25)	2.717(1)	2.515(16)	2.31	3.63
11	2.484(30)		2.531(12)	2.33	3.66
12	2.492(36)		2.537(6)	2.36	3.63
13	2.493(42)			2.38	

TABLE V. Average homonuclear and heteronuclear interatomic distances (in angstrom) and average Co and Fe magnetic moments (in μ_B) of the lowest energy homotopes of the biplanar hcp 13-atom CoFe nanoalloys as a function of the number of Co atoms. In parenthesis is shown the number of nearest neighbors bonds.

Co atoms	Co-Co	Fe-Fe	Co-Fe	μ(Co)	μ(Fe)
0		2.520(36)			3.08
1		2.535(32)	2.377(4)	2.06	3.08
2		2.540(25)	2.418(11)	1.84	3.12
3		2.577(24)	2.388(12)	2.16	3.25
4		2.577(15)	2.388(21)	2.16	3.25
5	2.441(7)	2.547(14)	2.430(15)	1.89	3.20
6	2.440(9)	2.563(12)	2.498(15)	1.93	3.20
7	2.458(12)	2.544(6)	2.424(18)	1.92	3.26
8	2.432(15)	2.532(4)	2.437(17)	1.95	3.29
9	2.426(18)	2.565(2)	2.436(16)	1.98	3.30
10	2.420(21)		2.449(15)	2.00	3.32
11	2.420(26)		2.444(10)	2.03	3.32
12	2.420(31)		2.449(5)	2.06	3.33
13	2.419(36)			2.08	

bution of Co and Fe atoms of the corresponding homotopes illustrated in Fig. 5. For intermediate and larger concentrations we obtain a mixed character with more layerlike order in some concentrations. The situation for the hcp nanoalloy is less clear. Most points lie between the segregated and the mixed ideal models, with several intermediate concentrations lying close to the layerlike behavior as illustrated in Fig. 6(b).

Coming now to the local magnetic properties, the icosahedral nanoalloys behave in general as the five-atom ones with regard to the slight enhancement of the local moments when increasing the Co concentration, which is reflected in the average Co and Fe moments. In the hcp nanoalloys the tendency is verified only in the rich Co phase ($x \geq 0.54$). We note that in the low Co phase, the chemical order in the hcp nanoalloys is also less clear than in the icosahedral ones. In Tables IV and V we report the interatomic distances and average Co and Fe moments for the icosahedral and the hcp nanoalloys, respectively.

V. SUMMARY

The main conclusions of* our DFT calculations of the $(Co_xFe_{1-x})_N$ ($N=5$ and 13) nanoalloys as a function of the relative composition are as follows. (i) The most stable five-atom Fe-Co nanoalloy is found at 40% of Co. (ii) We predict a transition from icosahedral to biplanar hcp structure in the $N=13$ nanoalloy as going from the Fe-rich phase to the Co-rich phase at about 50%–60% of Co, although the most stable composition corresponds to pure Co_{13}. (iii) We obtain ferromagneticlike coupling, with high average magnetic moments which decrease, in general, in 1 μ_B/N as increasing the Co concentration due to the substitution of Fe atoms by Co ones having one less d hole. (iv) Despite the above decrease in the average magnetic moment, we find a slight enhancement of the local Co and Fe magnetic moments as increasing the Co concentration. This trend already exists in the CoFe dimer. (v) We find a tendency to segregate for both low and rich Co concentrations and a slight tendency to mix for the intermediate concentration region. For the 13-atom icosahedral nanoalloy, we find that the Co atoms occupy the central site. The biplanar hcp nanoalloys have more tendency to segregate than the icosahedral ones. But since these sizes are small and most atoms are surfacelike, only qualitative trends can be inferred with regard to the chemical order.

Our results illustrate the rich structural and magnetic behavior of the Fe-Co alloys at the nanoscale. We hope that our study will stimulate future experimental works on these binary magnetic particles which could be interesting for high-density magnetic storage devices.

ACKNOWLEDGMENTS

We acknowledge the financial support from PROMEP (Contract No. SEP-CA230), CONACyT (Contract No. 2005–50650), and Spanish Ministry of Science and Innovation (Project No. FIS2008-02490/FIS) in conjunction with the European Regional Development Fund and by the Junta de Castilla y León (Grant No. GR120). Computer resources from the Centro Nacional de Supercomputo (CNS) from the IPICyT, San Luis Potosí (S.L.P.), México are acknowledged.

[1] R. Hong, N. O. Fisher, T. Emrick, and V. M. Rotello, Chem. Mater. **17**, 4617 (2005); W. R. Lee, M. G. Kim, J. R. Choi, J. Park, S. J. Koo, S. J. Oh, and J. Cheon, J. Am. Chem. Soc. **127**, 16090 (2005).

[2] M. H. Shao, K. Sasaki, and R. R. Adzic, J. Am. Chem. Soc. **128**, 3526 (2006); W. Q. Tian, M. Ge, F. Gu, T. Yamada, and Y. Aoki, J. Phys. Chem. A **110**, 6285 (2006); X. Q. Li and W. X. Zhang, Langmuir **22**, 4638 (2006).

[3] P. Crespo, M. A. García, E. Fernández Pinel, M. Multigner, D. Alcántara, J. M. de la Fuente, S. Penadés, and A. Hernando, Phys. Rev. Lett. **97**, 177203 (2006); H. L. Nguyen, L. E. M. Howard, G. W. Stinton, S. R. Giblin, B. K. Tanner, I. Terry, A. K. Hughes, I. M. Ross, A. Serres, and J. S. O. Evans, Chem. Mater. **18**, 6414 (2006); G. Ennas, A. Falqui, G. Paschina, and G. Marongiu, *ibid.* **17**, 6486 (2005).

[4] P. Gambardella, S. Rusponi, M. Veronese, S. S. Deshi, C. Grazioli, A. Dallmeyer, I. Cabria, R. Zeller, P. H. Dederichs, K. Kern, C. Carbone, and H. Brune, Science **300**, 1130 (2003); T. Jamneala, V. Madhavan, and M. F. Crommie, Phys. Rev. Lett. **87**, 256804 (2001); S. Pick, V. S. Stepanyuk, A. L. Klavsyuk, L. Niebergall, W. Hergert, J. Kirschner, and P. Bruno, Phys. Rev. B **70**, 224419 (2004); S. Heinrichs, W. Dieterich, and P. Maass, *ibid.* **75**, 085437 (2007).

[5] E. K. Parks, K. P. Kerns, and S. J. Riley, Chem. Phys. **262**, 151 (2000).

[6] R. Ferrando, A. Fortunelli, and G. Rossi, Phys. Rev. B **72**, 085449 (2005); J. Guevara, A. M. Llois, and M. Weissmann, Phys. Rev. Lett. **81**, 5306 (1998).

[7] D. Zitoun, M. Respaud, M. C. Fromen, M. J. Casanove, P. Lecante, C. Amiens, and B. Chaudret, Phys. Rev. Lett. **89**, 037203 (2002); C. Antoniak, J. Lindner, M. Spasova, D. Sudfeld, M. Acet, M. Farle, K. Fauth, U. Wiedwald, H.-G. Boyen, P. Ziemann, F. Wilhelm, A. Rogalev, and S. Sun, *ibid.* **97**, 117201 (2006).

[8] G. Mpourmpakis, G. E. Froudakis, A. N. Andriotis, and M. Menon, Phys. Rev. B **72**, 104417 (2005).

[9] J. M. Soler, E. Artacho, J. D. Gale, A. García, J. Junquera, P. Ordejoón, and D. Sánchez-Portal, J. Phys.: Condens. Matter **14**, 2745 (2002).

[10] J. P. Perdew, K. Burke, and M. Ernzerhof, Phys. Rev. Lett. **77**, 3865 (1996).

[11] N. Troullier and J. L. Martins, Phys. Rev. B **43**, 1993 (1991).

[12] L. Kleinman and D. M. Bylander, Phys. Rev. Lett. **48**, 1425 (1982).

[13] J. Izquierdo, A. Vega, L. C. Balbas, D. Sanchez-Portal, J. Junquera, E. Artacho, J. M. Soler, and P. Ordejon, Phys. Rev. B **61**, 13639 (2000).

[14] O. Diéguez, M. M. G. Alemany, C. Rey, P. Ordejón, and L. J. Gallego, Phys. Rev. B **63**, 205407 (2001).

[15] M. Castro, C. Jamorsky, and D. R. Salahub, Chem. Phys. Lett. **271**, 133 (1997).

[16] Q.-M. Ma, Z. Xie, J. Wang, and Y.-Ch. Li, Solid State Commun. **142**, 114 (2007).

[17] P. A. Montano and G. K. Shenoy, Solid State Commun. **35**, 53 (1980).

[18] H. Purdum, P. A. Montano, G. K. Shenoy, and T. Morrison, Phys. Rev. B **25**, 4412 (1982); D. M. Cox, D. J. Trevor, R. L. Whetten, E. A. Rohlfing, and A. Kaldor, *ibid.* **32**, 7290 (1985); S. S. Lin and A. Kant, J. Phys. Chem. **73**, 2450 (1969); I. Shim and K. A. Gingerich, J. Chem. Phys. **77**, 2490 (1982); L. Lian, C.-X. Su, and P. B. Armentrout, *ibid.* **97**, 4072 (1992).

[19] Q.-M. Ma, Z. Xie, J. Wang, Y. Liu, and Y.-Ch., Phys. Lett. A **358**, 289 (2006).

[20] G. Rollmann, P. Entel, and S. Sahoo, Comput. Mater. Sci. **35**, 275 (2006).

[21] S. Datta, M. Kabir, S. Ganguly, B. Sanyal, T. Saha-Dasgupta, and A. Mookerjee, Phys. Rev. B **76**, 014429 (2007).

[22] C. D. Dong and X. G. Gong, Phys. Rev. B **78**, 020409(R) (2008).

[23] H. J. Fan, C. W. Liu, and M. S. Liao, Chem. Phys. Lett. **273**, 353 (1997).

[24] F. Y. Liu, F. X. Li, and P. B. Armentrout, J. Chem. Phys. **123**, 064304 (2005).

[25] A. Kant and B. Strauss, J. Chem. Phys. **41**, 3806 (1964).

[26] D. A. Hales, C.-X. Su, Li Lian, and P. B. Armentrout, J. Chem. Phys. **100**, 1049 (1994).

[27] X. Xu, S. Yin, R. Moro, and W. A. de Heer, Phys. Rev. Lett. **95**, 237209 (2005).

[28] M. B. Knickelbein, J. Chem. Phys. **125**, 044308 (2006).

[29] F. Ducastelle, in *Order and Phase Stability in Alloys*, edited by F. R. de Boer and D. G. Petiffor (North Holland, Amsterdam, 1991).